



Universiteit  
Leiden  
The Netherlands

## **Caging ruthenium complexes with non-toxic ligands for photoactivated chemotherapy**

Cuello Garibo, J.A.

### **Citation**

Cuello Garibo, J. A. (2017, December 19). *Caging ruthenium complexes with non-toxic ligands for photoactivated chemotherapy*. Retrieved from <https://hdl.handle.net/1887/58688>

Version: Not Applicable (or Unknown)

License: [Licence agreement concerning inclusion of doctoral thesis in the Institutional Repository of the University of Leiden](#)

Downloaded from: <https://hdl.handle.net/1887/58688>

**Note:** To cite this publication please use the final published version (if applicable).

Cover Page



Universiteit Leiden



The handle <http://hdl.handle.net/1887/58688> holds various files of this Leiden University dissertation.

**Author:** Cuello Garibo J.A

**Title:** Caging ruthenium complexes with non-toxic ligands for photoactivated chemotherapy

**Issue Date:** 2017-12-19

# 5

## Tuning the stereoselectivity, photoreactivity, and redox potential of cycloruthenated complexes by small changes in the N,S ligand

*Cycloruthenated complexes may have more potential as anti-cancer agents than their non-cyclometalated analogues due to favorable charge, lipophilicity, and electrochemical properties. Their general red shift in the absorption spectrum makes them promising complexes for Photoactivated Chemotherapy (PACT). However, cycloruthenated complexes usually do not substitute a ligand upon light irradiation. In this chapter, we report the synthesis and photochemistry of four cyclometalated ruthenium complexes having the formula  $[Ru(bpy)(phpy)(L)]PF_6$  ( $bpy = 2,2'$ -bipyridine and  $phpy = 2$ -phenylpyridine) in which  $L$  is either 3-(methylthio)propylamine ( $mtpa$ ,  $[2]PF_6$ ), 2-(methylthio)ethylamine ( $mtea$ ,  $[3]PF_6$ ), 2-(methylthio)ethyl-2-pyridine ( $mtep$ ,  $[4]PF_6$ ), or 2-(methylthio)methylpyridine ( $mtmp$ ,  $[5]PF_6$ ). We show that the stereoselectivity of the synthesis, the photoreactivity, and the electrochemical properties depend critically on the size of the N,S chelating ring and the nature of the nitrogen ligand – primary amine vs. pyridine.*

This chapter is to be submitted as a full paper: J. A. Cuello-Garibo, C. James, S. L. Hopkins, M. A. Siegler, S. Bonnet, *in preparation*.

## 5.1 Introduction

Cyclometalated complexes are complexes containing a metallacycle in which at least one of the donor atoms in the first coordination sphere is either an  $sp^2$  or an  $sp^3$  carbon. In the last two decades cycloruthenated complexes have been intensively studied for Grätzel-type dye-sensitized solar cells (DSSCs) and for anticancer therapy.<sup>1-3</sup> In the latter, they show, in general, higher cytotoxicity *in vitro* compared to their non-cyclometalated analogues.<sup>3-4</sup> This higher cytotoxicity may be due to the higher lipophilicity of the complexes, which allows a higher cellular uptake, and a lower  $Ru^{III/II}$  redox potential, which causes interactions with proteins such as oxido-reductase enzymes.<sup>5</sup> These advantages, together with their ability to generate reactive oxygen species (ROS) upon light irradiation, make them good candidates for Photodynamic Therapy (PDT).<sup>6</sup> Furthermore, the destabilization of the  $t_{2g}$  orbitals of the ruthenium(II) center due to the strong  $\pi$ -donor character of the metal-bound carbon atom in, for example, the chelate 2-phenylpyridine (phpy<sup>-</sup>), shifts the metal-to-ligand charge transfer (<sup>1</sup>MLCT) absorption band to lower energies compared to non-cyclometalated analogues.<sup>2</sup> This property is particularly relevant in the phototherapy field, in which photoactive complexes should absorb light, if possible, in the phototherapeutic window (700 – 1000 nm) which penetrates deep enough in biological tissues. However, in the field of Photoactivated Chemotherapy (PACT), an oxygen-independent therapy that relies on the activation of a prodrug by exchange of one or more of the ligands upon light irradiation, the impact of cycloruthenated complexes in the literature is still scarce due to their often limited photoreactivity. Destabilization of the  $e_g$  orbitals of the ruthenium(II) center compared to non-cyclometalated analogues increases the gap between the  $\pi^*$  orbital of the ligand and the  $e_g$  orbital and thus makes the thermal population of the <sup>3</sup>MC excited state from the <sup>3</sup>MLCT more difficult,<sup>7-8</sup> which is at the basis of ligand photosubstitution reactions in octahedral  $d^6$  metal complexes.<sup>9-11</sup> In non-cyclometalated complexes a common strategy to enhance photoreactivity is to lower the energy of the <sup>3</sup>MC by using hindering polypyridyl ligands and increasing the octahedral distortion.<sup>12-13</sup> However, this strategy proved not to be useful in the case of  $[Ru(biq)_2(phpy)]PF_6$  (biq = 2,2'-biquinoline), as this complex is neither photoreactive in  $CH_3CN$  nor in water upon green light irradiation.<sup>14</sup> To date, only a few cyclometalated ruthenium compounds have been reported that release one of the ligands upon light irradiation. One of the first examples of a light-activatable cyclometalated ruthenium complex, discovered by Pfeffer *et al.*<sup>3</sup> and later studied more in detail by Turro *et al.*, is  $[Ru(phen)(phpy)(CH_3CN)_2]PF_6$  (phen = 1,10-phenanthroline, [**1a**] $PF_6$ ), which photosubstitutes one  $CH_3CN$  by a  $Cl^-$  in  $CH_2Cl_2$  in

the presence of 2 mM of TBACl. When OVCAR-5 cells were treated with this complex, EC<sub>50</sub> values of 1 μM and 70 nM were found in the dark and upon light irradiation, respectively, with a photo index (PI) of 14.<sup>15</sup>

In Chapter 3 we demonstrated that upon light irradiation polypyridyl complexes such as [Ru(bpy)<sub>2</sub>(mtmp)]<sup>2+</sup> (bpy = 2,2'-bipyridine; mtmp = 2-(methylthio)methylpyridine) or [Ru(Ph<sub>2</sub>phen)<sub>2</sub>(mtmp)]<sup>2+</sup> (Ph<sub>2</sub>phen = 4,7-diphenyl-1,10-phenanthroline) will substitute the non-cytotoxic N,S ligand mtmp by two water molecules. While complexes bearing two bpy ligands generally did not show any cytotoxicity against lung cancer cells (A549 cells) due to their high hydrophilicity and low cellular uptake, complexes with two Ph<sub>2</sub>phen ligands showed low EC<sub>50</sub> values after irradiation, but were already toxic in the dark (EC<sub>50</sub> = 2.7 μM), probably due to their high lipophilicity.<sup>16</sup> These results led us to wonder whether it would be possible to synthesize a photoactivatable cyclometalated complex that, upon light irradiation, photosubstitutes a bidentate N,S chelate such as mtmp. In this chapter, we report the synthesis and properties of four cyclometalated complexes having the formula [Ru(bpy)(phpy)(L)]PF<sub>6</sub>, in which L is either 3-(methylthio)propylamine (mtpa, [2]PF<sub>6</sub>), 2-(methylthio)ethylamine (mtea, [3]PF<sub>6</sub>), 2-(methylthio)ethyl-2-pyridine (mtep, [4]PF<sub>6</sub>), or mtmp ([5]PF<sub>6</sub>). In particular, the stereoselectivity of the synthesis and the photoreactivity were found to depend critically on both the size of the the N,S chelate ring and the nature of the nitrogen ligand – primary amine vs. pyridine.

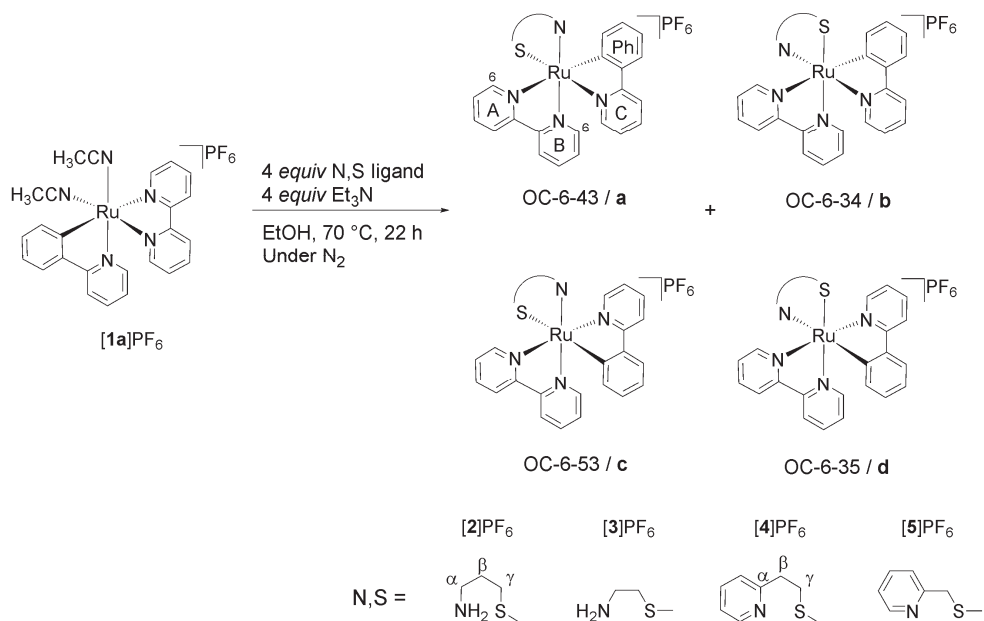
## 5.2 Results

### 5.2.1 Stereoselectivity of the synthesis

The four cycloruthenated complexes [2]PF<sub>6</sub> – [5]PF<sub>6</sub> were prepared as shown in Scheme 5.1, following the synthetic route established by the group of Michel Pfeiffer.<sup>17-18</sup> The dimer [(η<sup>6</sup>-C<sub>6</sub>H<sub>6</sub>)RuCl(μ-Cl)]<sub>2</sub> was heated in CH<sub>3</sub>CN at 45 °C together with NaOH, KPF<sub>6</sub>, and Hphpy to yield the cycloruthenated complex [Ru(phpy)(CH<sub>3</sub>CN)<sub>4</sub>]PF<sub>6</sub>. After purification by column chromatography on alumina using CH<sub>2</sub>Cl<sub>2</sub> as eluent, the complex was further reacted with 0.8 equiv of bpy in CH<sub>2</sub>Cl<sub>2</sub> at room temperature for 20 h to obtain *cis*-[Ru(bpy)(phpy)(CH<sub>3</sub>CN)<sub>2</sub>]PF<sub>6</sub> ([1a]PF<sub>6</sub>), with the carbon donor atom *trans* to bpy. Achieving the controlled coordination of only one equivalent of bpy is not straightforward, as formation of [Ru(bpy)<sub>2</sub>(phpy)]PF<sub>6</sub> easily occurs in this reaction. To avoid formation of this product, only 0.8 equiv of bpy was added to the reaction mixture. As shown by Ryabov *et al.* only the isomer having the σ-bound C atom *trans* to bpy ([1a]PF<sub>6</sub>) was obtained.<sup>19</sup>

Coordination of the third ligand (*i.e.* mtpa, mtea, mtep, or mtmp) was performed under identical conditions, which consisted in heating the precursor [**1a**]PF<sub>6</sub> at 70 °C in EtOH in presence of *ca.* 4 equiv of the N,S ligand and 4 equiv of Et<sub>3</sub>N (to ensure coordination of the amine of the N,S ligand) for 22 h under Ar. After crystallization by vapour diffusion of diethyl ether into the crude mixture, yields between 44% and 58% were obtained for complexes [**2**]PF<sub>6</sub>, [**3**]PF<sub>6</sub>, [**4**]PF<sub>6</sub>, and [**5**]PF<sub>6</sub>. Interestingly, synthesis of complexes [**2**]PF<sub>6</sub> and [**3**]PF<sub>6</sub> was attempted several times since in many occasions a dark green solid was obtained, which is believed to be an oxidized ruthenium(III) species. This did not happen when synthesizing complexes [**4**]PF<sub>6</sub> and [**5**]PF<sub>6</sub>, which already indicates the strong influence of the nature of the nitrogen ligand of the N,S chelate on the properties of the cyclometalated complexes.

Octahedral complexes bearing three different bidentate ligands, two of which are dissymmetric, potentially have many isomers. The carbon donor atom can be either *trans* or *cis* to the nitrogen donor atoms of the bpy ligand, and in each of these cases the nitrogen of the N,S ligand can be *trans* to either the bpy or to the phpy<sup>-</sup> ligand, leading to up to four coordination isomers, each of which exists as an enantiomeric pair  $\Lambda/\Delta$  (Scheme 5.1). Following the IUPAC configuration index convention, these four coordination isomers are named (OC-6-43)-[Ru(bpy)(phpy)(N,S)]PF<sub>6</sub>, (OC-6-34)-[Ru(bpy)(phpy)(N,S)]PF<sub>6</sub>, (OC-6-53)-[Ru(bpy)(phpy)(N,S)]PF<sub>6</sub>, and (OC-6-35)-[Ru(bpy)(phpy)(N,S)]PF<sub>6</sub>, but for an easier reading in this chapter we will name them isomers **a**, **b**, **c**, and **d**, respectively (Scheme 5.1). Next to the different configurations of the coordination sphere created by the dissymmetry of the ligands, the coordinating sulfur atom is a prochiral center that, after coordination to ruthenium, can adopt either an *R* or an *S* configuration. Thus, for each of the four  $\Lambda$  coordination isomers a pair of diastereoisomers  $\Lambda$ -*R* and  $\Lambda$ -*S* may exist, obtaining a total of eight possible  $\Lambda$ -isomers for [**3**]<sup>+</sup> and [**5**]<sup>+</sup>. Finally, in the case of complexes [**2**]<sup>+</sup> and [**4**]<sup>+</sup>, the N,S chelate creates a six-membered ring that can switch between two chair conformations where the methyl group of the thioether is either in equatorial (*eq*) or in axial (*ax*) position depending on the conformation of the chair (see Scheme 4.1 and Chapter 4). These configurations are not identical, and there are hence 16 possible  $\Lambda$ -isomers for these two complexes.



Scheme 5.1. Synthesis of  $[2]PF_6$ ,  $[3]PF_6$ ,  $[4]PF_6$ , and  $[5]PF_6$  and the four possible regioisomers. For clarity only the  $\Lambda$  isomers are shown, but all samples were obtained as racemic  $\Delta/\Lambda$  mixtures.

In spite of the high number of possible isomers for these molecules,  $[2]PF_6$  and  $[4]PF_6$  were obtained as single  $\Lambda/\Delta$  enantiomeric pair of isomers according to the  $^1H$  NMR spectra in acetone- $d_6$ . Characteristic doublets for H in the 6 position on the bpy were found to be at 9.82 and 9.44 ppm for  $[2]PF_6$  and  $[4]PF_6$ , respectively, as shown in Figure 5.1a and Figure 5.1c. Single sets of peaks in the aromatic region corresponding to 16 and 20 H were found, respectively. Mass spectrometry of  $[2]PF_6$  and  $[4]PF_6$  showed peaks at 517.1 and 565.5, respectively, corresponding to  $[2]^+$  (calcd  $m/z$  = 517.1) and  $[4]^+$  (calcd  $m/z$  = 565.1). On the other hand, as shown in Figure 5.1b, the  $^1H$  NMR spectrum of  $[3]PF_6$  in acetone- $d_6$  showed two doublets at 9.02 and 9.11 ppm in an integration ratio of 1:0.8. Mass spectrometry showed a single peak at  $m/z$  = 503.5 corresponding to  $[3]^+$  (calcd  $m/z$  = 503.1), which means that the two sets of NMR peaks belong to two different isomers. A similar situation was observed for complex  $[5]PF_6$ , with three doublets in the  $^1H$  NMR spectrum at 9.16, 9.39, and 9.49 ppm in a ratio of 0.3:1:0.2 (Figure 5.1d). Mass spectrometry also showed a single peak at  $m/z$  = 552.1 corresponding to  $[5]^+$  (calcd  $m/z$  = 551.1), indicating the formation of three isomers out of the eight possible. Overall, despite the apparent complexity of this synthesis, the right number of carbon atoms (*i.e.* three) between the N and the S atoms of the N,S chelate allows to prepare the tris-heteroleptic cyclometalated complexes

[2]PF<sub>6</sub> and [4]PF<sub>6</sub> stereoselectively, *i.e.* as a single pair of  $\Lambda/\Delta$  enantiomers, while a shorter chain (two carbon atoms) leads to mixtures of isomers in [3]PF<sub>6</sub> and [5]PF<sub>6</sub>.

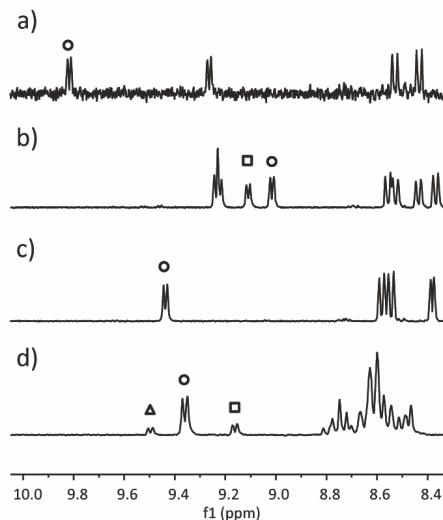


Figure 5.1. <sup>1</sup>H NMR of solutions of [2]PF<sub>6</sub> (a), [3]PF<sub>6</sub> (b), [4]PF<sub>6</sub> (c), and [5]PF<sub>6</sub> (d) in acetone-*d*<sub>6</sub>. Peaks corresponding to the H at position 6 on the bpy of the major isomer are marked with a circle, and the peaks corresponding to the H at position 6 on the bpy of the second and third isomers (if any) are marked with a square and triangle, respectively.

### 5.2.2 Structural characterization (DFT, NOESY, and X-Ray)

The identification of the configuration of these complexes is challenging, and only [2]PF<sub>6</sub> and [4]PF<sub>6</sub> were studied further, since they were obtained as single isomers. First, Density Functional Theory (DFT) minimization of the isomers of both complexes was performed in water using the COSMO model to simulate solvent effects (see Experimental Section). In each case only the  $\Lambda$  enantiomers with the six-membered chelate ring in a chair conformation were modelled. The sulfur atom was placed either in the *R* or *S* configuration. To reduce the amount of structures to be optimized, only the isomers with the methyl group in an equatorial position were calculated (see Chapter 4). The optimized structures and their energies in water are given in Figure AVI.5, Figure AVI.6, and in Table 5.1, respectively. For [2]<sup>+</sup>, the isomer  $\Lambda$ -(*S*)-*eq*-[2d]<sup>+</sup> was found to be the most stable, with the other isomers at energies ranging from +2.6 to +10.0 kJ·mol<sup>-1</sup> (Table 5.1). Although the energy differences are relatively small, it is clear that the thermodynamically most stable isomer is  $\Lambda$ -(*S*)-*eq*-[2d]<sup>+</sup>, which has the  $\sigma$ -bound C atom *trans* to the amine of mtpa. For complex [4]<sup>+</sup>, isomer  $\Lambda$ -(*S*)-*eq*-[4d]<sup>+</sup> was also found to be the most stable in water, followed by the other *S*

isomers at energies ranging from +8.8 to 10.6 kJ·mol<sup>-1</sup>, and then the *R* isomers at energies ranging from +10.9 to +21.2 kJ·mol<sup>-1</sup> (Table 5.1). In this case, the energy differences between the most and least stable isomers are significantly larger than for [2]<sup>+</sup>, which highlights the different geometric requirements of the sp<sup>2</sup> carbon and nitrogen atoms in [4]<sup>+</sup> vs. that of the sp<sup>3</sup> atoms in [2]<sup>+</sup>. Notably, the six-membered ring involving the mtep ligand was found to be in a *pseudo-chair* conformation in the minimized structures, due to the different orbital hybridization of the N and C atoms of the pyridine ring. For example, in  $\Lambda$ -(*S*)-*eq*-[4d]<sup>+</sup> the angle C<sub>β</sub>-C<sub>α</sub>-N is 120.17°, whereas in  $\Lambda$ -(*S*)-*eq*-[2d]<sup>+</sup> it is 113.54°. Another potential reason for the increased stabilization of isomer **d** of [4]<sup>+</sup> is that the electron-rich carbon ligand is *trans* to the π-accepting pyridine ligand of mtep, while in [2d]<sup>+</sup> the *trans* primary amine cannot accept the excess electron density. Overall, all the isomers of both complexes with the sulfur in *R* configuration and the methyl group in equatorial position show very short distances between that methyl group and the closest proton at position 6 on bpy or phpy<sup>-</sup> (~ 2.1 Å, Table 5.1), whereas with the *S* configuration that distance is much longer (~ 3.5 Å, Table 5.1). In the latter configuration, the methyl group sits above the middle of either the bpy or the phpy<sup>-</sup> ligands (called ancillary ligands), lowering steric repulsions and thus explaining the general preference for an *S* configuration of the sulfur atom. Although the structures having the methyl group in axial position were not minimized, a similar trend is expected. As explained in Chapter 4 (Scheme 4.1), the inversion of the *pseudo-chair* does not change the configuration of the sulfur atom but it changes the position of the methyl group from equatorial to axial and *vice versa*. This inversion does not affect the position of the methyl group with respect to the ancillary ligands and their corresponding steric effects.

Table 5.1. Absolute and relative energies in water (COSMO) of the isomers of [2]<sup>+</sup> and [4]<sup>+</sup> optimized by DFT/PBE0/TZP, and distances (Å) between H of the N,S ligand and the spatially closest H<sub>6</sub> of the ancillary ligands.

	Absolute energy in water (Hartree)	Relative energy ΔE in water (kJ.mol <sup>-1</sup> )	SCH <sub>3</sub> ...H <sub>6</sub>	H <sub>γ</sub> ...H <sub>6</sub>	H <sub>β</sub> ...H <sub>6</sub>
Λ-(R)-eq-[2a] <sup>+</sup>	-16.34735195	10.0	2.0901	2.0916	3.2482
Λ-(R)-eq-[2b] <sup>+</sup>	-16.34749222	9.6	2.2032	2.1088	3.3374
Λ-(R)-eq-[2c] <sup>+</sup>	-16.34868079	6.5	2.1478	2.2332	3.0378
Λ-(R)-eq-[2d] <sup>+</sup>	-16.34791025	8.5	2.1245	2.0899	3.1498
Λ-(S)-eq-[2a] <sup>+</sup>	-16.34864080	6.6	3.6948	2.9525	3.2417
Λ-(S)-eq-[2b] <sup>+</sup>	-16.34956230	4.2	3.7037	2.0800	3.1900
Λ-(S)-eq-[2c] <sup>+</sup>	-16.35015479	2.6	3.8634	3.0299	3.1182
Λ-(S)-eq-[2d] <sup>+</sup>	-16.35015479	0.0	3.8355	2.8732	3.1084
Λ-(R)-eq-[4a] <sup>+</sup>	-17.90977751	21.2	2.0115	2.335	2.4537
Λ-(R)-eq-[4b] <sup>+</sup>	-17.91011750	20.3	2.026	2.6181	2.3643
Λ-(R)-eq-[4c] <sup>+</sup>	-17.91162229	16.3	2.0457	2.6024	2.3409
Λ-(R)-eq-[4d] <sup>+</sup>	-17.91370630	10.9	2.0361	2.2468	2.4817
Λ-(S)-eq-[4a] <sup>+</sup>	-17.91402838	10.0	3.282	3.3278	2.2499
Λ-(S)-eq-[4b] <sup>+</sup>	-17.91448159	8.8	3.5303	3.0197	2.3136
Λ-(S)-eq-[4c] <sup>+</sup>	-17.91378390	10.6	3.4180	3.1008	2.2527
Λ-(S)-eq-[4d] <sup>+</sup>	-17.91783987	0.0	3.4844	2.909	2.3536

In order to see whether this theoretical result is confirmed by experiments, <sup>1</sup>H NMR studies in acetone-d<sub>6</sub> were performed to assign the structure of the species in solution. Unfortunately, the instability and easy degradation of compound [2]PF<sub>6</sub> made the acquisition of a high-quality NOESY spectrum impossible, making the detection of the main off-diagonal signals challenging. However, COSY, HSQC, and NOESY spectroscopy of [4]PF<sub>6</sub> in acetone-d<sub>6</sub> at room temperature allowed for the assignment of the peaks corresponding to the three ligands. The NOESY spectrum showed equivalent off-diagonal signals between A6 of bpy and H<sub>γ</sub> of mtep and between H<sub>β</sub> and A6 of bpy and C6 of phpy<sup>-</sup> (Figure 5.2a). The DFT modelled structures showed that signals between A6 and H<sub>β</sub> and H<sub>γ</sub> of mtep are unlikely in the same complex due to the great difference of both distances in every modelled isomer (Figure 5.2b). NOESY studies at 193 K were performed to detect inversion of the coordinated sulfur atom. At such temperature, the off-diagonal signal between A6 and H<sub>γ</sub> is much weaker than that

between C6 and H<sub>β</sub>, and the off-diagonal signal between A6 and H<sub>β</sub> is not present (Figure 5.2c). All the DFT modelled structures with the sulfur atom in *R* configuration were discarded since, together with those signals, a stronger signal between the thioether methyl group and A6 should be observed due to the short distance between those atoms (~2 Å) (Figure 5.2 and Table 5.1). Among the other isomers, the one that fits best with the reported off-diagonal signals is  $\Lambda$ -(*S*)-*eq*-[4c]<sup>+</sup> (with sulfur *trans* to the  $\sigma$ -bound C), with distances between A6 and H<sub>γ</sub> and between C6 and H<sub>β</sub> of 3.101 and 2.253 Å, respectively. Isomer  $\Lambda$ -(*S*)-*ax*-[4d]<sup>+</sup> would also fit with the reported off-diagonal signals, although not modelled with DFT. Single crystals suitable for X-Ray structure determination were obtained for complexes [4]PF<sub>6</sub> by slow vapor diffusion of diethyl ether into a solution of the complex in acetone. The crystal structure is a racemate of a single isomer of [Ru(bpy)(phpy)(mtep-κN,κS)]PF<sub>6</sub> in an orthorhombic P<sub>2</sub>12<sub>1</sub>1 space group, containing both configurations  $\Lambda$ -(*S*) and  $\Delta$ -(*R*) with the pyridine of the N,S ligand *trans* to the  $\sigma$ -bound C donor atom and the methyl group in a *pseudo*-axial position. Thus, the obtained structure corresponds to the isomer  $\Lambda$ -(*S*)-*ax*-[4d]PF<sub>6</sub>, confirming the geometry predicted by NOESY studies in solution. The structure, shown in Figure 5.3, shows a longer Ru-S bond (2.3331(8) Å) compared to the Ru-N bonds of the ancillary ligands (between 2.049(2) and 2.085(2) Å), as expected from the higher ionic radius of sulfur compared to nitrogen. The Ru-N bond (2.239(3) Å) *trans* to the Ru-C bond (2.027(3) Å) is also significantly longer than the other Ru-N bonds, which fits with the expected *trans* influence of the electron-rich carbon donor atom.

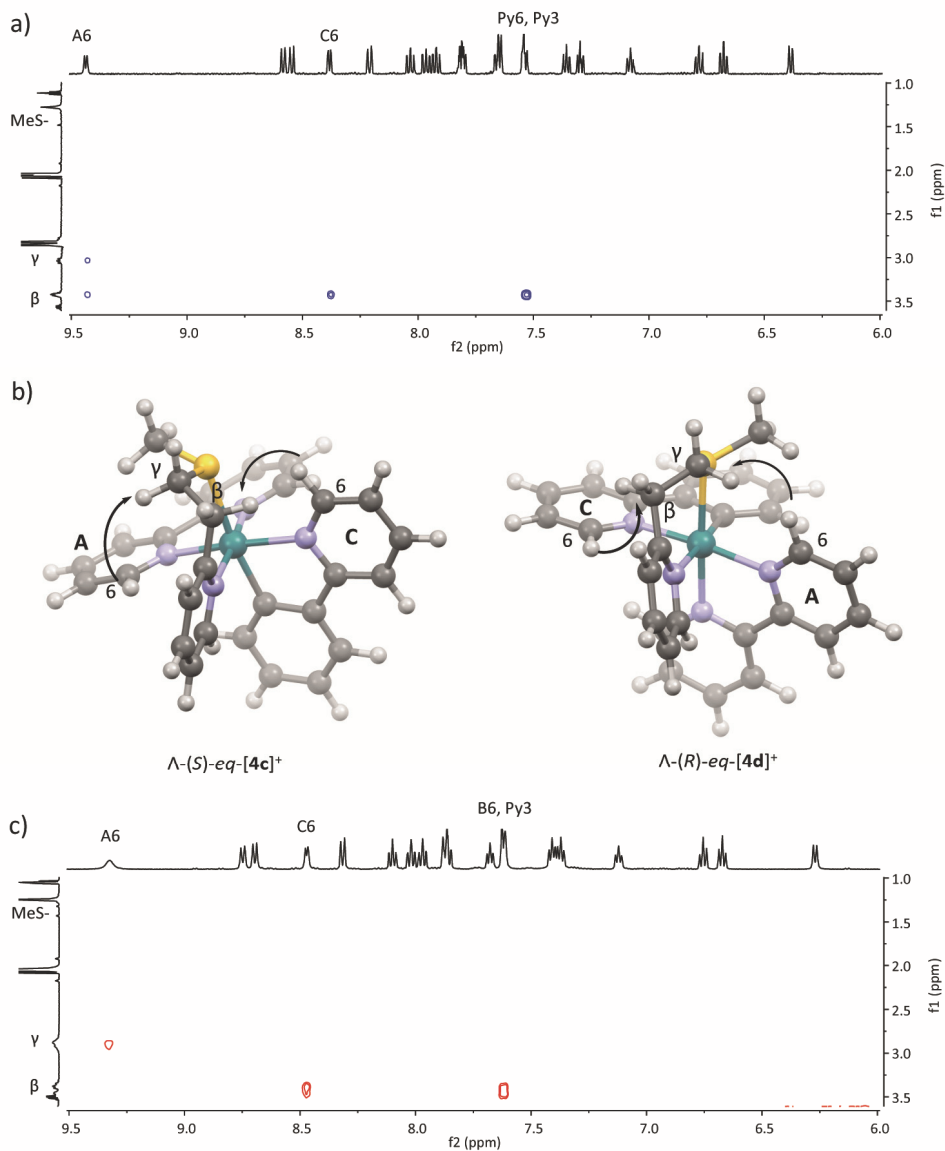


Figure 5.2. NOESY spectra of acetone- $d_6$  solution of  $[4]PF_6$  at 293 K (a) showing off-diagonal signals between  $H_\beta$  and C6,  $H_\beta$  and A6, and  $H_\gamma$  and A6. At 193 K (c), the off-diagonal signal between  $H_\beta$  and A6 is not visible. b) Isomers  $\Lambda$ -(S)-eq-[4c]<sup>+</sup> and  $\Lambda$ -(R)-eq-[4d]<sup>+</sup> modelled by DFT show the short distances between  $H_\beta$  and C6 (2.2527 and 2.4817 Å, respectively) and  $H_\gamma$  and A6 (3.1008 and 2.2468 Å, respectively), thus these isomers would fit with the NOESY signals. However, in  $\Lambda$ -(R)-eq-[4d]<sup>+</sup> an interaction between  $CH_3S$ - and A6 should be also visible due to the short distance (2.0361 Å).

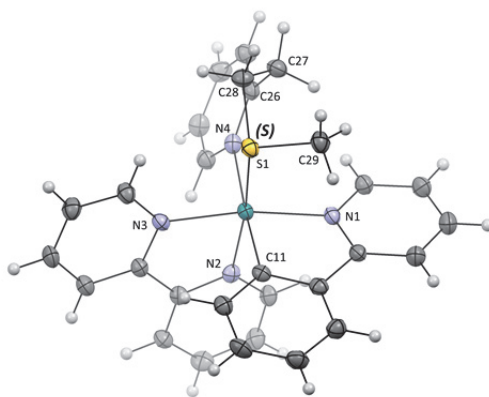


Figure 5.3. Displacement ellipsoid plot (50% probability level) of the  $\Delta$  enantiomer of the cationic complex in the crystal structure of the pair  $\Delta$ -(S)/ $\Delta$ -(R)-ax-[4d]PF<sub>6</sub>. The hexafluoridophosphate counteranion has been omitted for clarity.

Table 5.2. Selected bond length (Å) and angles (°) for  $\Delta$ -(S)/ $\Delta$ -(R)-ax-[4d]PF<sub>6</sub>.

$\Delta$ -(S)-ax-[4d]PF <sub>6</sub>	
<b>Ru1-S1</b>	2.3310(8)
<b>Ru1-N1</b>	2.085(2)
<b>Ru1-N2</b>	2.060(2)
<b>Ru1-N3</b>	2.049(2)
<b>Ru1-N4</b>	2.239(3)
<b>Ru1-C11</b>	2.027(3)
<b>S1-C28-C26-N4</b>	26.4(2)

### 5.2.3 Electronic spectroscopy and electrochemistry

The UV-vis absorption spectra in CH<sub>3</sub>CN of compounds [2]PF<sub>6</sub> – [5]PF<sub>6</sub> are provided in Figure 5.4 and their absorption maxima ( $\lambda_{\text{max}}$ ) and molar extinction coefficients ( $\epsilon$ ) are listed in Table 5.3. It must be noted that for complexes [3]PF<sub>6</sub> and [5]PF<sub>6</sub>, mixtures of two or three isomers were used. A common feature in all the absorption spectra is the presence of two main bands in the MLCT region: one with a  $\lambda_{\text{max}}$  around 390 nm and a broader band between 450 and 650 nm with a lower molar absorption coefficient, with the tail of the band reaching the 700 nm region. According to Bomben *et al.* the first band corresponds to a <sup>1</sup>MLCT transition involving the coordinated carbon atom of the phpy<sup>-</sup> ligand, whereas the broad band at a lower energy corresponds to a Ru→bpy transition.<sup>2</sup> This broad MLCT band compared to the non-cyclometalated analogues is a result of the lower symmetry of the cyclometalated compound.<sup>2</sup> The lower-energy MLCT band has a  $\lambda_{\text{max}}$  of 530 and 540 nm for primary amine-based complexes [2]PF<sub>6</sub>

and [3]PF<sub>6</sub>, respectively, whereas pyridine-based complexes [4]PF<sub>6</sub> and [5]PF<sub>6</sub> show a blue-shifted band with  $\lambda_{\text{max}}$  at 526 and 501 nm, respectively. Furthermore, the latter two compounds show bands with a shoulder, which could be ascribed to an overlapping Ru→py transition. For complex [2]PF<sub>6</sub> a band with  $\lambda_{\text{max}}$  at 725 nm is also visible, however, this band may be the result of oxidation of the complex. The degradation of [2]PF<sub>6</sub> may also explain the much lower molar absorption coefficient of the Ru→phpy<sup>-</sup> band of complex [2]PF<sub>6</sub> (6900 M<sup>-1</sup>·cm<sup>-1</sup>) compared to the other three complexes (around 10000 M<sup>-1</sup>·cm<sup>-1</sup>).

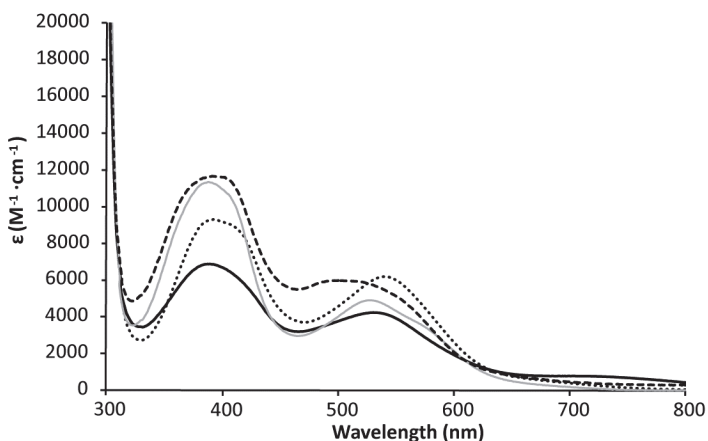


Figure 5.4. Electronic absorption spectra of solutions in CH<sub>3</sub>CN of [2]PF<sub>6</sub> (black continuous), [3]PF<sub>6</sub> (dots), [4]PF<sub>6</sub> (grey continuous), and [5]PF<sub>6</sub> (dashes).

The electrochemical properties of complexes [2]PF<sub>6</sub> – [5]PF<sub>6</sub> were investigated using cyclic voltammetry in CH<sub>3</sub>CN in order to gain more insight on the redox stability of these complexes (Figure AVI.1). For complexes [2]PF<sub>6</sub> and [3]PF<sub>6</sub> the reversible oxidation wave corresponding to the Ru<sup>III</sup>/Ru<sup>II</sup> couple is observed at a potential  $E_{1/2}$  of -0.03 and 0.00 V vs. Fc<sup>+0</sup>, respectively, whereas complexes [4]PF<sub>6</sub> and [5]PF<sub>6</sub> show a reversible peak at a significantly higher potential  $E_{1/2}$  of +0.16 V vs. Fc<sup>+0</sup> (Table 5.3), highlighting the  $\pi$ -acceptor properties of the pyridine-based N,S chelating ligand, which stabilizes the HOMO of complexes [4]PF<sub>6</sub> and [5]PF<sub>6</sub> compared to that of [2]PF<sub>6</sub> and [3]PF<sub>6</sub>. In practice, the oxidation of the former compounds is more difficult, which makes them stable in air, while compounds [2]PF<sub>6</sub> and [3]PF<sub>6</sub> are easily oxidized during their synthesis. Small changes of the N,S ligand can thus have significant consequences on the applicability of a cyclometalated complex.

Table 5.3. Wavelength of MLCT transition ( $\lambda_{\text{abs}}/\text{nm}$ ) and molar absorptivity ( $\epsilon/\text{M}^{-1}\cdot\text{cm}^{-1}$ ) of [2]PF<sub>6</sub>, [3]PF<sub>6</sub>, [4]PF<sub>6</sub>, and [5]PF<sub>6</sub> in CH<sub>3</sub>CN. Redox potentials of [2]PF<sub>6</sub>, [3]PF<sub>6</sub>, [4]PF<sub>6</sub>, and [5]PF<sub>6</sub> as measured by cyclic voltammetry.<sup>a</sup>

Complex	$\lambda_{\text{abs}}/\text{nm}$ ( $\epsilon/\text{M}^{-1}\cdot\text{cm}^{-1}$ )	$E_{1/2}(\text{Ru}^{\text{III/II}})/\text{V}^{\text{a}}$	$\Delta E_{\text{p}}/\text{V}^{\text{a}}$
[Ru(bpy)(phpy)(mtpa)]PF <sub>6</sub> [2]PF <sub>6</sub>	530 (4300), 389 (6900)	-0.03	0.060
[Ru(bpy)(phpy)(mtea)]PF <sub>6</sub> [3]PF <sub>6</sub> <sup>b</sup>	540 (6200), 392 (9300)	0.00	0.071
[Ru(bpy)(phpy)(mtep)]PF <sub>6</sub> [4]PF <sub>6</sub>	526 (4900), 388 (11400)	+0.16	0.060
[Ru(bpy)(phpy)(mtmp)]PF <sub>6</sub> [5]PF <sub>6</sub> <sup>c</sup>	501 (6000), 395 (11700)	+0.16	0.090

<sup>a</sup> Measurement conditions: 1 mM of the complexes in 0.1 M Bu<sub>4</sub>NPF<sub>6</sub>/CH<sub>3</sub>CN, scanning rate 100 mV·s<sup>-1</sup>. The potentials are referenced to Fc<sup>+1/0</sup>; <sup>b</sup>A mixture of two isomers in a ratio 1:0.8 was used; <sup>c</sup>A mixture of three isomers in a ratio 0.3:1:0.2 was used.

## 5.2.4 Thermal stability and photochemistry

The thermal stability in the dark of all four complex was studied in CH<sub>3</sub>CN using UV-vis spectroscopy. Under air, solutions in CH<sub>3</sub>CN of complexes [2]PF<sub>6</sub>, [3]PF<sub>6</sub>, [4]PF<sub>6</sub>, and [5]PF<sub>6</sub> did not show any significant changes in the UV-vis spectra over time, except for a general increase in the absorbance due to evaporation of the solvent (Figure AVI.3a-d). Thus, in CH<sub>3</sub>CN in the dark no oxidation nor thermal substitution of the N,S ligand by solvent molecules occurred.

The photoreactivity of the complexes was studied in CH<sub>3</sub>CN and monitored with UV-vis spectroscopy, mass spectrometry, and NMR spectroscopy. When a solution of [3]PF<sub>6</sub> in CH<sub>3</sub>CN was irradiated with a green (521 nm) LED at a photon flux of  $\sim 6 \cdot 10^{-8}$  mol·s<sup>-1</sup> under Ar, the UV-vis spectra did not show any change of the absorption bands. Only a general increase of the absorbance was observed due to the slow evaporation of the solvent (Figure 5.5b). Thus, [3]PF<sub>6</sub> is not photoreactive in CH<sub>3</sub>CN. However, when a solution of [2]PF<sub>6</sub> in CH<sub>3</sub>CN was irradiated under the same conditions, the UV-vis spectra showed a small shift of the  $\lambda_{\text{max}}$  of both MLCT bands from 534 nm and 388 nm to 518 nm and 378 nm, respectively, with isosbestic points at 421 nm and 552 nm (Figure 5.5a). Although the photoreaction did not reach a steady state, mass spectrometry after 3 h of irradiation showed a peak at  $m/z = 494.1$ , corresponding to [Ru(bpy)(phpy)(CH<sub>3</sub>CN)<sub>2</sub>]<sup>+</sup> (calcd  $m/z = 494.1$ ), proving that photosubstitution of mtpa by two solvent molecules occurred. Furthermore, irradiation of an acetonitrile solution of [4]PF<sub>6</sub> under the same conditions showed a similar hypsochromic shift of the maximum absorption of both MLCT bands from 526 nm and 388 nm to 516 nm and 376 nm, respectively, reaching a steady state after 6 h (Figure 5.5c). Mass spectrometry at that point showed the peak of the bis-acetonitrile photoproduct at  $m/z = 494.1$ , thus photosubstitution of mtep by two solvent molecules

occurred as well. Since complex  $[4]PF_6$  is the only air-stable complex of the series that was obtained as a pure single isomer, the quantum yield of the photoreaction could be determined. Using Glotaran global fitting, the quantum yield for the photosubstitution of mtep ( $\Phi_{PR}$ ) was calculated to be 0.00035 (see Appendix I and Figure AVI.2), which is ten times lower than the  $\Phi_{PR}$  for the irradiation of  $[Ru(bpy)_2(mtmp)]Cl_2$  in water (0.0030, see Chapter 3). Finally, irradiation of a solution of  $[5]PF_6$  showed a very slow change in the UV-vis spectra over time with a shift of the MLCT bands to the blue with isosbestic points at 474 nm and 546 nm (Figure 5.5d). Although the photoreaction did not reach a steady state, mass spectrometry after 15 h irradiation also showed a peak at  $m/z = 494.1$ . Thus, complexes  $[2]PF_6$ ,  $[4]PF_6$ , and  $[5]PF_6$  proved to be photoreactive and lead to the same photoproduct, *i.e.*  $[Ru(bpy)(phpy)(CH_3CN)_2]^+$ , although the rate of the photoreaction of  $[5]PF_6$  was much lower than that of the two other complexes.

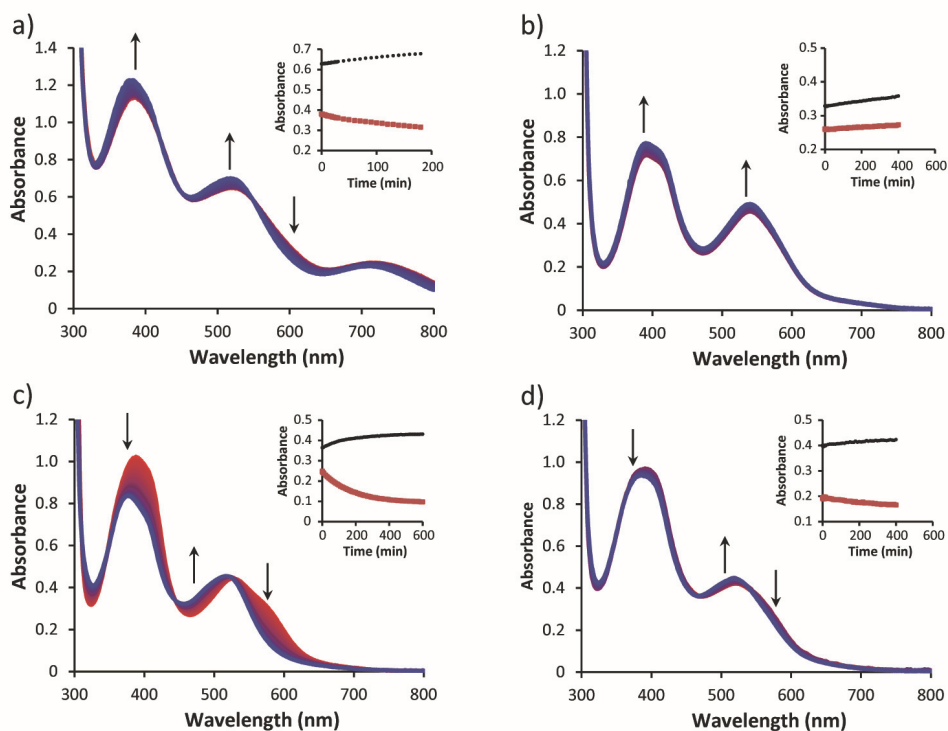
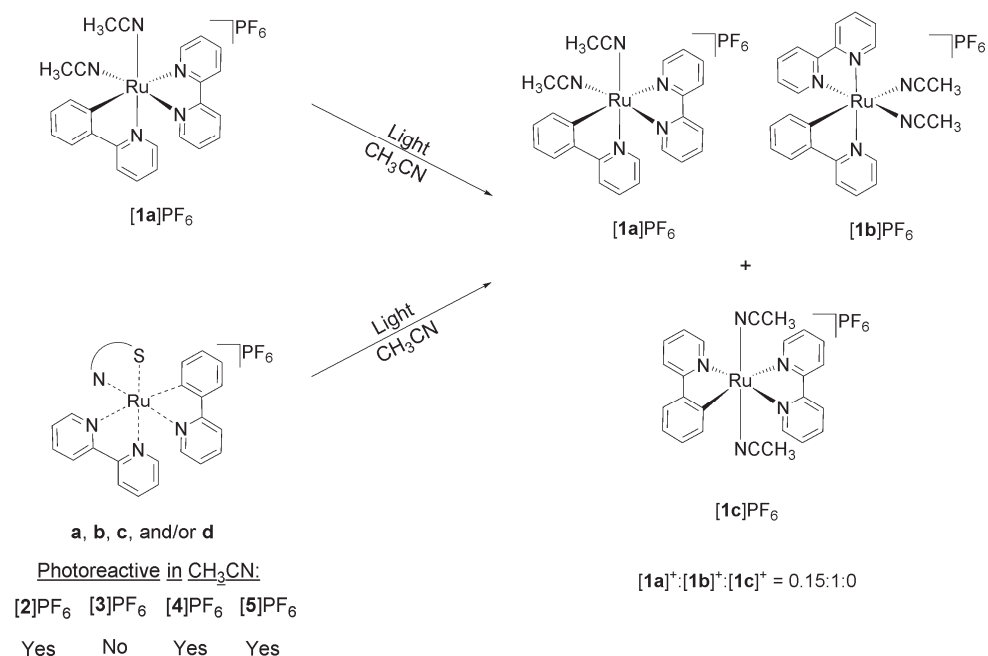
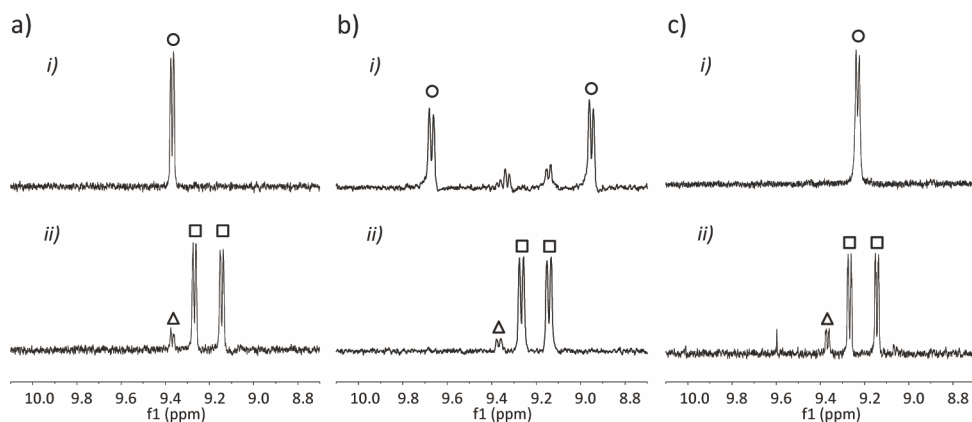


Figure 5.5. Evolution of the UV-vis spectra of  $CH_3CN$  solutions of a)  $[2]PF_6$  (0.151 mM), b)  $[3]PF_6$  (0.093 mM), c)  $[4]PF_6$  (0.094 mM), and d)  $[5]PF_6$  (0.101 mM) upon irradiation with a 521 nm LED (photon fluxes of  $8.62 \cdot 10^{-8}$ ,  $6.09 \cdot 10^{-8}$ ,  $6.80 \cdot 10^{-8}$ , and  $6.17 \cdot 10^{-8} \text{ mol} \cdot \text{s}^{-1}$ , respectively) under  $N_2$ . Inset: black dots represent the absorbance at 500 nm vs. time, and red squares represent the absorbance at 590 nm vs. time.

In order to determine which isomer of the photoproduct was obtained, the photoreactivity of complexes  $[2]PF_6$  and  $[4]PF_6$  was studied with  $^1H$  NMR in  $CD_3CN$  by irradiation with a 1000 W Xe lamp fitted with a long pass 400 nm and an IR filter. As shown in Figure 5.6b, after 6 h irradiation of a solution of  $[2]PF_6$ , the doublets at 8.95 and 9.67 ppm disappeared, whereas new doublets at 9.37, 9.26, and 9.14 ppm arose in a ratio 0.13:1:1. The same species were obtained after 1.5 h irradiation of complex  $[4]^+$  under the same conditions (Figure 5.6c). However, only the doublet at 9.37 ppm corresponds to  $[Ru(bpy)(phpy)(CH_3CN)_2]^+$  with the coordinated carbon *trans* to bpy ( $[1a]^+$ ),<sup>19</sup> which is obtained as the minor compound in the steady state. Thus, to which isomer do the other two doublets correspond? Thermal and photochemical isomerization of  $[1a]^+$  into the isomer with the coordinated carbon atom *trans* to  $CH_3CN$  ( $[1b]^+$ ) was already reported by Pfeffer *et al.* (Scheme 5.2).<sup>18</sup> However, the reported  $^1H$  NMR shifts did not fit with our NMR data. In order to study which photoproduct was obtained, a solution of  $[1a]PF_6$  in  $CD_3CN$  was irradiated under the same conditions as complexes  $[2]PF_6$  and  $[4]PF_6$ . As shown in Figure 5.6a, after 5 h the doublet at 9.37 ppm had decreased in intensity and two new doublets arose at 9.26 and 9.14 ppm reaching a steady state between both isomers with a ratio 0.16:1, thus showing that the same photoproducts were obtained in this experiment as upon irradiation of  $[2]PF_6$  and  $[4]PF_6$ . However, due to the exchange of coordinated  $CH_3CN$  by  $CD_3CN$ , the peaks belonging to the coordinated  $CH_3CN$  molecules were not visible in  $^1H$  NMR, making the assignment of the stereochemistry of these photoproducts impossible. Thus, the photoreaction was performed in  $CH_3CN$ , the solvent was removed by rotary evaporation at 20 °C, and the crude product was redissolved in  $CDCl_3$  to analyze it by  $^1H$  NMR. The spectrum showed a doublet at 9.48 ppm integrating for one H and two singlets at 2.31 and 2.27 ppm integrating for three protons each, which were assigned to the coordinated  $CH_3CN$  molecules (Figure AVI.4). The isomer with both  $CH_3CN$  molecules *trans* to each other and the polypyridyl ligands in the equatorial plane ( $[1c]PF_6$ ) was discarded as a possible photoproduct since both  $CH_3CN$  molecules would be equivalent, thus resulting in one singlet integrating for 6 protons. This control experiment only leaves one possible isomer as a photoproduct for the irradiation of  $[1a]PF_6$ ,  $[2]PF_6$ , and  $[4]PF_6$ , *i.e.* the *cis* isomer  $[1b]PF_6$  (Scheme 5.2).



*Scheme 5.2. Summary of the products obtained upon irradiation of CH<sub>3</sub>CN solutions of complexes [1a]PF<sub>6</sub>, [2]PF<sub>6</sub>, [3]PF<sub>6</sub>, [4]PF<sub>6</sub>, and [5]PF<sub>6</sub> performed either with a 521 nm LED with a photon flux of  $\sim 7 \cdot 10^{-8} \text{ mol} \cdot \text{s}^{-1}$  (0.1 mM) and monitored with UV-vis spectroscopy, or with a Xe lamp (2 mM) and monitored with <sup>1</sup>H NMR. According to <sup>1</sup>H NMR a mixture of isomers [1a]<sup>+</sup>:[1b]<sup>+</sup> in a ratio of  $\sim 0.15:1$  was always obtained, with no presence of the trans isomer [1c]<sup>+</sup>. For clarity, only the *A* isomers are shown, but all samples were obtained as racemic  $\Delta/\Lambda$  mixtures.*



*Figure 5.6. Evolution of the <sup>1</sup>H NMR spectra (region 10.0 – 8.8 ppm) of a solution in CD<sub>3</sub>CN of a) [1a]PF<sub>6</sub> (2.61 mM), b) [2]PF<sub>6</sub> (4.47 mM), and c) [4]PF<sub>6</sub> (1.84 mM) irradiated with a 1000 W Xe lamp fitted with a 400 nm long pass filter and an IR filter. i) At *t* = 0, ii) at *t* = 5 h (a), *t* = 6 h (b), and *t* = 1.5 h (c). Circles: starting product, squares: [1b]<sup>+</sup>, triangles: [1a]<sup>+</sup>.*

### 5.3 Discussion

In the literature it is generally accepted that in complexes of the type  $[\text{Ru}(\text{bpy})(\text{phpy})(\text{N},\text{N})]^+$ , synthesized from  $[\text{Ru}(\text{bpy})(\text{phpy})(\text{CH}_3\text{CN})_2]^+$ , the third bidentate N,N ligand coordinates to ruthenium by simply substituting the  $\text{CH}_3\text{CN}$  molecules without isomerization, *i.e.* *cis* to the carbon donor atom of  $\text{phpy}^-$ .<sup>20</sup> However, Pfeffer *et al.* recently showed that this structural assignment might not be correct.<sup>18</sup>  $\text{CH}_3\text{CN}$  is a very good ligand for ruthenium(II) and in order to turn it into a good leaving group the complex must first isomerize (either thermally or photochemically) so that one  $\text{CH}_3\text{CN}$  becomes *trans* to the carbon ligand, which is a very reactive position due to the *trans* effect of the C donor atom.<sup>18</sup> This mechanism seems to occur also for the coordination of the N,S ligands, as the obtained isomer in  $[\mathbf{4}]^+$  has the N atom of the last incoming ligand *trans* to the carbon atom of  $\text{phpy}^-$ , as proven by NOESY studies and the X-Ray structure. Furthermore, although all the complexes are stable in  $\text{CH}_3\text{CN}$  solution under air, we observed during the synthesis that complexes bearing a primary amine-based N,S ligand oxidized easier than compounds with a pyridine-based N,S ligand. Indeed, cyclic voltammetry of the four complexes showed a lower oxidation potential for  $[\mathbf{2}]\text{PF}_6$  and  $[\mathbf{3}]\text{PF}_6$  than for  $[\mathbf{4}]\text{PF}_6$  and  $[\mathbf{5}]\text{PF}_6$ . We suggest that the *trans* influence of the  $\sigma$ -bound C atom plays an important role in the oxidation. The  $\pi$ -accepting nature of the pyridine of the N,S ligand in  $[\mathbf{4}]\text{PF}_6$  and  $[\mathbf{5}]\text{PF}_6$  stabilizes the HOMO by accepting electron-density of the C donor atom in *trans* position, whereas primary amine-based ligands do not allow this, making the complexes more prone to oxidation. The higher energy of the MLCT band, *i.e.* the higher gap between the HOMO and the LUMO, of  $[\mathbf{4}]\text{PF}_6$  and  $[\mathbf{5}]\text{PF}_6$  compared to  $[\mathbf{2}]\text{PF}_6$  and  $[\mathbf{3}]\text{PF}_6$  is another sign of the stabilization of the HOMO for the pyridine-based complexes.

With regard to the photoreactivity, as explained in the Introduction, cycloruthenated complexes generally are not photoreactive, and the ones that are photoreactive are those which photosubstitute only one monodentate ligand. However, we found that six-membered rings like those found in  $[\mathbf{2}]^+$  and  $[\mathbf{4}]^+$  lower the ligand field splitting of the complexes and thus the energy of the  $^3\text{MC}$  levels well enough to recover photoreactivity in  $\text{CH}_3\text{CN}$ , without the necessity of adding hindering ligands. By contrast, N,S complexes with five-membered rings, such as  $[\mathbf{3}]^+$  and  $[\mathbf{5}]^+$ , were found to be either not photoreactive at all ( $[\mathbf{3}]^+$ ) or with only very low photoconversion rates ( $[\mathbf{5}]^+$ ). We suggest that these low photosubstitution rates are due to fast rechelation (also called recaptation) of the five-membered ring, like it occurs in the case of

$[\text{Ru}(\text{bpy})_3]^{2+}$  or  $[\text{Ru}(\text{bpy})_2(\text{glutamate-}\kappa\text{N},\kappa\text{O})]^{2+}$ .<sup>21-22</sup> Furthermore, whereas the NMR shifts of  $[\mathbf{1a}]^+$  correspond to those reported by Pfeffer *et al.* in 2005,<sup>19</sup> the NMR shifts of  $[\mathbf{1b}]^+$ , *i.e.* the isomer obtained after irradiation of  $[\mathbf{1a}]^+$ , do not correspond to those reported by Pfeffer *et al.* in 2013.<sup>18</sup> Nevertheless, as shown in the Results section, the identity of  $[\mathbf{1b}]^+$  is unequivocally assigned.

## 5.4 Conclusions

In this work, we have discovered that the ring size resulting from the coordination of an N,S ligand to ruthenium has a critical influence on the number of isomers obtained during the synthesis of  $[\mathbf{2}]^+ - [\mathbf{5}]^+$ , as well as on their photoreactivity. Under the same conditions tris-heteroleptic complexes bearing a six-membered ring ( $[\mathbf{2}]\text{PF}_6$  and  $[\mathbf{4}]\text{PF}_6$ ), in spite of their apparent configurational complexity, were obtained stereoselectively as a single couple of enantiomers  $\Lambda/\Delta$ , which in the case of  $[\mathbf{4}]\text{PF}_6$  could be assigned to  $\Lambda$ -(*S*)/ $\Delta$ -(*R*)-*ax*- $[\mathbf{4d}]\text{PF}_6$ . However, the complexes with five-membered N,S chelate rings were obtained as mixtures of isomers that could not be separated. This result opens new possibilities for the stereoselective synthesis of tris-heteroleptic ruthenium complexes bearing chiral and dissymmetric ligands. Complexes with a six-membered N,S chelate ring showed selective substitution of the N,S ligand in  $\text{CH}_3\text{CN}$  upon green light irradiation, since rechelation is apparently slow. Finally, cyclometallated complexes are electron rich, but their sensitivity to oxidation can be fine-tuned by using  $\pi$ -accepting pyridyl-containing bidentate ligands *trans* to the carbon donor atom, stabilizing the high electron density brought by cyclometalation. Thus, going away from polypyridyl ligands can be highly beneficial, both on the synthetic point of view and on the point of view of the photoreactivity, provided that the stereochemical complexity brought by the dissymmetric metallacycling ligands can be controlled by choosing the appropriate size of the ring resulting of the coordination of the N,S ligand. Overall, the novel complex  $[\mathbf{4}]\text{PF}_6$  fulfills all criteria to become a promising PACT agent: it can be synthesized in a stereoselectively manner, it is stable under  $\text{O}_2$ , and it photosubstitutes efficiently the non-toxic N,S ligand by two  $\text{CH}_3\text{CN}$  molecules. Biological studies are currently ongoing to assess the actual biological activity of this compound.

## 5.5 Experimental

### 5.5.1 Synthesis

**General:** The ligands 2-(methylthio)ethylamine (mtea), and 3-(methylthio)-propylamine (mtpa) were purchased from Sigma-Aldrich, as well as bis-[(benzene)dichlororuthenium] ( $[\eta^6\text{-}(\text{C}_6\text{H}_6)\text{RuCl}_2]_2$ ) and sodium hydroxide (NaOH). 2-Phenylpyridine (phpy), 2,2'-bipyridine (bpy), and potassium hexafluoridophosphate ( $\text{KPF}_6$ ) were purchased from Alfa-Aesar. All reactants and solvents were used without further purification. The synthesis of  $[\text{Ru}(\text{phpy})(\text{CH}_3\text{CN})_4]\text{PF}_6$ ,  $[\text{Ru}(\text{bpy})(\text{phpy})(\text{CH}_3\text{CN})_2]\text{PF}_6$  (**[1a]** $\text{PF}_6$ ), 2-(methylthio)methylpyridine (mtmp), and 2-(methylthio)ethyl-2-pyridine (mtep) were carried out according to literature procedures.<sup>17, 19, 23</sup>

Electrospray mass spectra (ES MS) were recorded by using a MSQ Plus Spectrometer. UV-vis spectra were recorded on a Cary Varian spectrometer. All  $^1\text{H}$  NMR spectra were recorded on a Bruker DPX-300 or DMX-400 spectrometers. Chemical shifts are indicated in ppm relative to the residual solvent peak.

**Synthesis of complexes [2] $\text{PF}_6$ , [3] $\text{PF}_6$ , [4] $\text{PF}_6$ , and [5] $\text{PF}_6$ .** General procedure: In a two-neck flask, a solution of **[1a]** $\text{PF}_6$  (1 equiv), N,S ligand (4 equiv), and  $\text{Et}_3\text{N}$  (4 equiv) were dissolved in deaerated EtOH (2 to 5 mL) and heated in an oil bath at 70 °C for 22 h under  $\text{N}_2$ . Then, a schlenk flask containing diethyl ether was attached to the flask containing the reaction mixture in order to obtain a crystalline dark precipitate by slow vapour diffusion. The solid was filtered, washed with diethyl ether, and stored at -20 °C.

**$[\text{Ru}(\text{bpy})(\text{phpy})(\text{mtpa})]\text{PF}_6$  (**[2]** $\text{PF}_6$ ).** According to the general procedure, a solution of **[1]** $\text{PF}_6$  (40 mg, 0.063 mmol), mtpa (28  $\mu\text{L}$ , 0.25 mmol), and  $\text{Et}_3\text{N}$  (40 mg, 0.29 mmol) in EtOH (5 mL) was heated at 70 °C for 22 h under  $\text{N}_2$ . After 6 days of slow vapour diffusion of diethyl ether into the EtOH solution, a crystalline dark precipitate was obtained (23 mg, 52%).  $^1\text{H}$  NMR (300 MHz, acetone- $d_6$ )  $\delta$  = 9.81 (dt,  $J$  = 5.8, 1.1 Hz, 1H), 9.26 (ddd,  $J$  = 5.7, 1.6, 0.8 Hz, 1H), 8.52 (dt,  $J$  = 8.2, 1.2 Hz, 1H), 8.43 (dt,  $J$  = 8.1, 1.1 Hz, 1H), 8.16 (dt,  $J$  = 8.1, 1.1 Hz, 1H), 8.07 – 8.02 (m, 1H), 7.97 (ddd,  $J$  = 8.2, 7.3, 1.6 Hz, 1H), 7.81 (ddd,  $J$  = 8.2, 7.5, 1.5 Hz, 1H), 7.74 (ddd,  $J$  = 8.8, 7.5, 1.4 Hz, 2H), 7.67 (dd,  $J$  = 5.7, 0.8 Hz, 1H), 7.46 (ddd,  $J$  = 7.2, 5.7, 1.4 Hz, 1H), 7.24 (ddd,  $J$  = 7.3, 5.7, 1.4 Hz, 1H), 6.73 – 6.66 (m, 1H), 6.59 (td,  $J$  = 7.3, 1.4 Hz, 1H), 6.40 (dd,  $J$  = 7.4, 1.2 Hz, 1H), 1.15 (s, 3H). High Resolution ES MS  $m/z$  (calcd):

517.09851 (517.09944, [2]<sup>+</sup>). UV-vis  $\lambda$  in nm ( $\epsilon$  in  $M^{-1}.cm^{-1}$ ): 530 (4300), 389 (6900) in  $CH_3CN$ .

**[Ru(bpy)(phpy)(mtea)]PF<sub>6</sub> ([3]PF<sub>6</sub>)**. According to the general procedure, a solution of [1]PF<sub>6</sub> (15 mg, 0.024 mmol), mtea (8.5  $\mu$ L, 0.095 mmol), and Et<sub>3</sub>N (7.0  $\mu$ L, 0.095 mmol) in EtOH (2 mL) was heated at 70 °C for 22 h under N<sub>2</sub>. After 5 days of slow vapour diffusion of diethyl ether into the EtOH solution, a crystalline dark precipitate was obtained (9.0 mg, 58%). Two isomers A/B in a ratio 1:0.8 were obtained. <sup>1</sup>H NMR (400 MHz, acetone-d<sub>6</sub>)  $\delta$  9.26 – 9.19 (m, 1H<sub>A</sub> + 1H<sub>B</sub>), 9.11 (d,  $J$  = 5.1 Hz, 1H<sub>B</sub>), 9.02 (d,  $J$  = 5.8 Hz, 1H<sub>A</sub>), 8.56 (d,  $J$  = 8.0 Hz, 1H<sub>A</sub>), 8.53 (d,  $J$  = 8.0 Hz, 1H<sub>B</sub>), 8.44 (dt,  $J$  = 6.5, 1.0 Hz, 1H<sub>B</sub>), 8.37 (dt,  $J$  = 8.0, 1.2 Hz, 1H<sub>A</sub>), 8.16 (d,  $J$  = 8.1 Hz, 1H<sub>B</sub>), 8.14 – 8.07 (m, 2H<sub>A</sub>), 8.05 – 8.00 (m, 1H<sub>B</sub>), 7.97 (ddd,  $J$  = 8.2, 7.3, 1.5 Hz, 1H<sub>B</sub>), 7.91 – 7.85 (m, 2H<sub>A</sub>), 7.83 (d,  $J$  = 5.8 Hz, 1H<sub>B</sub>), 7.82 – 7.73 (m, 2H<sub>A</sub> + 2H<sub>B</sub>), 7.71 – 7.64 (m, 1H<sub>A</sub> + 1H<sub>B</sub>), 7.43 (ddd,  $J$  = 7.2, 5.7, 1.4 Hz, 1H<sub>B</sub>), 7.38 (ddd,  $J$  = 7.3, 5.7, 1.5 Hz, 1H<sub>A</sub>), 7.22 (ddd,  $J$  = 7.3, 5.7, 1.4 Hz, 1H<sub>B</sub>), 7.11 (ddd,  $J$  = 7.3, 5.8, 1.4 Hz, 1H<sub>A</sub>), 6.77 (ddd,  $J$  = 7.7, 7.1, 1.4 Hz, 1H<sub>A</sub>), 6.74 – 6.67 (m, 1H<sub>A</sub> + 1H<sub>B</sub>), 6.64 (td,  $J$  = 7.3, 1.4 Hz, 1H<sub>B</sub>), 6.52 – 6.47 (m, 1H<sub>A</sub> + 1H<sub>B</sub>), 4.24 (d,  $J$  = 11.4 Hz, 1H), 4.12 (d,  $J$  = 12.1 Hz, 1H), 3.50 – 3.35 (m, 1H), 3.20 – 3.00 (m, 4H), 2.97 – 2.86 (m, 3H), 2.76 – 2.65 (m, 1H), 1.67 (s, 3H), 1.27 (s, 3H). High Resolution ES MS  $m/z$  (calcd): 503.08379 (503.08585, [3]<sup>+</sup>). UV-vis  $\lambda$  in nm ( $\epsilon$  in  $M^{-1}.cm^{-1}$ ): 540 (6200), 392 (9300) in  $CH_3CN$ .

**[Ru(bpy)(phpy)(mtep)]PF<sub>6</sub> ([4]PF<sub>6</sub>)**. According to the general procedure, a solution of [1]PF<sub>6</sub> (30 mg, 0.046 mmol), mtep (27 mg, 0.18 mmol), and Et<sub>3</sub>N (26  $\mu$ L, 0.19 mmol) in EtOH (5 mL) was heated at 70 °C for 22 h under N<sub>2</sub>. After 4 days of slow vapour diffusion of diethyl ether into the EtOH solution, a crystalline dark precipitate was obtained (14 mg, 44%). A pure single isomer was obtained. <sup>1</sup>H NMR (400 MHz, acetone-d<sub>6</sub>)  $\delta$  9.44 (d,  $J$  = 5.8 Hz, 1H, A6), 8.58 (dt,  $J$  = 7.9 Hz, 1H, A3), 8.54 (dt,  $J$  = 8.1, 1.1 Hz, 1H, B3), 8.38 (ddd,  $J$  = 5.7, 1.6, 0.8 Hz, 1H, C6), 8.21 (dt,  $J$  = 8.4, 1.2 Hz, 1H, C3), 8.06 – 8.00 (m, 1H, A4), 7.99 – 7.94 (m, 1H, C4), 7.94 – 7.88 (m, 1H, B4), 7.84 – 7.78 (m, 2H, Py5 + Ph3), 7.68 – 7.63 (m, 2H, A5 + B6), 7.56 – 7.51 (m, 2H, Py3 + Py6), 7.36 (ddd,  $J$  = 7.4, 5.7, 1.4 Hz, 1H, B5), 7.30 (ddd,  $J$  = 7.3, 5.7, 1.4 Hz, 1H, C5), 7.08 (ddd,  $J$  = 7.3, 5.7, 1.4 Hz, 1H, Py4), 6.78 (ddd,  $J$  = 7.7, 7.2, 1.3 Hz, 1H, Ph4), 6.68 (td,  $J$  = 7.3, 1.4 Hz, 1H, Ph 5), 6.42 – 6.36 (m, 1H, Ph6), 3.46 – 3.41 (m, 2H,  $\beta$ ), 3.09 – 2.99 (m, 2H,  $\gamma$ ), 1.28 (s, 3H, CH<sub>3</sub>S-). <sup>13</sup>C NMR (101 MHz, acetone-d<sub>6</sub>)  $\delta$  152.98, 152.33, 152.06, 150.15, 138.38, 137.17, 137.08, 135.80, 134.97, 128.95, 128.19, 127.52, 127.19, 124.72, 124.59, 124.43, 124.06, 123.46, 121.61,

120.16, 34.95, 32.00, 15.20. High Resolution ES MS  $m/z$  (calcd): 565.10083 (565.09944, [4]<sup>+</sup>). Anal. Calcd for C<sub>29</sub>H<sub>27</sub>F<sub>6</sub>N<sub>4</sub>PRuS: C, 49.08; H, 3.84; N, 7.90 Found: C, 48.84; H, 3.99; N, 7.65. UV-vis  $\lambda$  in nm ( $\epsilon$  in M<sup>-1</sup>.cm<sup>-1</sup>): 526 (4900), 388 (11300) in CH<sub>3</sub>CN.

**[Ru(bpy)(phpy)(mtmp)]PF<sub>6</sub>** ([5]PF<sub>6</sub>). According to the general procedure, a solution of [1]PF<sub>6</sub> (20 mg, 0.031 mmol), mtmp (17 mg, 0.12 mmol), and Et<sub>3</sub>N (20  $\mu$ L, 0.14 mmol) in EtOH (5 mL) was heated at 70 °C for 22 h under N<sub>2</sub>. After 5 days of slow vapour diffusion of diethyl ether into the EtOH solution, a crystalline dark precipitate was obtained (9.7 mg, 45%). <sup>1</sup>H NMR of 3 isomers labelled as A, B, and C (300 MHz, acetone-d<sub>6</sub>)  $\delta$  = 9.50 (d,  $J$  = 5.6 Hz, 1H<sub>A</sub>), 9.36 (dd,  $J$  = 5.5, 1.2 Hz, 1H<sub>B</sub>), 9.16 (d,  $J$  = 5.8 Hz, 1H<sub>B</sub>), 8.83 – 8.74 (m, 1H<sub>A</sub> + 1H<sub>C</sub>), 8.62 (dt,  $J$  = 7.4, 1.8 Hz, 2H<sub>B</sub>), 8.53 – 8.46 (m, 1H<sub>A</sub> + 1H<sub>C</sub>), 8.31 (d,  $J$  = 6.9 Hz, 1H<sub>C</sub>), 8.24 – 8.19 (m, 1H<sub>A</sub> + 1H<sub>B</sub> + 1H<sub>C</sub>), 8.17 – 8.09 (m, 1H<sub>C</sub>), 8.07 – 8.00 (m, 1H<sub>B</sub>), 8.02 – 7.93 (m, 1H<sub>A</sub> + 1H<sub>B</sub> + 1H<sub>C</sub>), 7.87 – 7.79 (m, 5H), 7.74 – 7.67 (m, 1H<sub>A</sub> + 1H<sub>C</sub>), 7.61 (ddd,  $J$  = 7.3, 5.8, 1.4 Hz, 1H<sub>B</sub>), 7.49 (d,  $J$  = 5.5 Hz, 1H<sub>B</sub>), 7.39 (ddd,  $J$  = 7.3, 5.7, 1.4 Hz, 1H<sub>B</sub>), 7.29 – 7.25 (m, 1H<sub>A</sub> + 1H<sub>C</sub>), 7.22 (t,  $J$  = 8.0 Hz, 1H<sub>B</sub>), 7.08 – 7.02 (m, 1H<sub>A</sub> + 1H<sub>C</sub>), 6.99 (d,  $J$  = 9.0 Hz, 1H<sub>A</sub>), 6.91 – 6.84 (m, 1H<sub>C</sub>), 6.83 – 6.76 (m, 1H<sub>B</sub>), 6.68 (td,  $J$  = 7.3, 1.4 Hz, 1H<sub>B</sub>), 6.48 (dd,  $J$  = 7.4, 1.3 Hz, 1H<sub>B</sub>), 6.42 (d,  $J$  = 6.8 Hz, 1H<sub>A</sub>). ES MS  $m/z$  (calcd): 551.1 (551.1, [5]<sup>+</sup>). UV-vis  $\lambda$  in nm ( $\epsilon$  in M<sup>-1</sup>.cm<sup>-1</sup>): 501 (6000), 395 (11700) in CH<sub>3</sub>CN.

### 5.5.2 Cyclic voltammetry

Electrochemical measurements were performed at room temperature under argon using an Autolab PGstat10 potentiostat controlled by NOVA software. A three-electrode cell system was used with a glassy carbon working electrode, a platinum counter electrode and an Ag/AgCl reference electrode. All electrochemistry measurements were done in CH<sub>3</sub>CN solution with tetrabutylammonium hexafluoridophosphate as the supporting electrolyte.

### 5.5.3 Photochemistry

**General:** For the irradiation experiments of NMR tubes, the light of a LOT 1000 W Xenon Arc lamp mounted with 400 nm long pass and IR filters was used. For NMR experiments under N<sub>2</sub>, NMR tubes with PTFE stopper were used. UV-vis experiments were performed on a Cary 50 Varian spectrometer. When following photoreactions by UV-vis and mass spectrometry, a LED light source ( $\lambda_{\text{ex}}$  = 521 nm, with a Full Width at

Half Maximum of 33 nm) with a photon flux between  $6.09$  and  $8.62 \cdot 10^{-8} \text{ mol} \cdot \text{s}^{-1}$  was used.

**Experiments monitored with  $^1\text{H}$  NMR:** A stock solution in  $\text{CD}_3\text{CN}$  of either  $[\mathbf{1a}]\text{PF}_6$  (2.61 mM),  $[\mathbf{2}]\text{PF}_6$  (4.47 mM) or  $[\mathbf{4}]\text{PF}_6$  (1.84 mM) was prepared and deaerated under  $\text{N}_2$ . Then, 660  $\mu\text{L}$  were transferred, under  $\text{N}_2$ , into a NMR tube. The tube was irradiated at room temperature with a LOT Xenon 1000 W lamp equipped with IR short pass and 400 nm long pass filters. In addition, a control experiment without white light irradiation was performed. The reactions were monitored with  $^1\text{H}$  NMR at various time intervals.

**Experiments monitored with UV-vis and MS:** UV-vis spectroscopy was performed using a UV-vis spectrometer equipped with temperature control set to 298 K and a magnetic stirrer. The irradiation experiments were performed in a quartz cuvette containing 3 mL of solution. A stock solution of the desired complex was prepared using  $\text{CH}_3\text{CN}$ , which was then diluted in the cuvette to a working solution concentration. When the experiment was carried out under  $\text{N}_2$  the sample was deaerated 15 min by gentle bubbling of  $\text{N}_2$  and the atmosphere was kept inert during the experiment by a gentle flow of  $\text{N}_2$  on top of the cuvette. A UV-vis spectrum was measured every 30 s for the first 10 min, every 1 min for the next 10 min, and eventually every 10 min until the end of the experiment. Data was analysed with Microsoft Excel. Experimental conditions are detailed in Table 5.4.

Table 5.4. Conditions of the photoreactions monitored with MS and UV-vis.

Complex	Stock solution			Working sol. (mM)	Photon flux ( $\text{mol} \cdot \text{s}^{-1}$ )
	w (mg)	V (mL)	M (mM)		
$[\mathbf{2}]\text{PF}_6$	1.0	10	0.151	0.151	$8.62 \cdot 10^{-8}$
$[\mathbf{3}]\text{PF}_6$	0.9	10	0.139	0.093	$6.09 \cdot 10^{-8}$
$[\mathbf{4}]\text{PF}_6$	1.0	10	0.141	0.094	$6.80 \cdot 10^{-8}$
$[\mathbf{5}]\text{PF}_6$	1.4	10	0.201	0.101	$6.17 \cdot 10^{-8}$

### 5.5.4 Single Crystal X-Ray crystallography

**General:** All reflection intensities were measured at 110(2) K using a SuperNova diffractometer (equipped with Atlas detector) with  $\text{Cu } K\alpha$  radiation ( $\lambda = 1.54178 \text{ \AA}$ ) under the program CrysAlisPro (Version CrysAlisPro 1.171.39.29c, Rigaku OD, 2017). The same program was used to refine the cell dimensions and for data reduction. The structure was solved with the program SHELXS-2014/7 and was

refined on  $F^2$  with SHELXL-2014/7.<sup>24</sup> Analytical numeric absorption correction based on a multifaceted crystal model was applied using CrysAlisPro. The temperature of the data collection was controlled using the system Cryojet (manufactured by Oxford Instruments). The H atoms were placed at calculated positions (unless otherwise specified) using the instructions AFIX 23, AFIX 43, or AFIX 137 with isotropic displacement parameters having values 1.2  $U_{eq}$  of the attached C atoms.

**Crystal growing:** [4]PF<sub>6</sub> (1.0 mg) was dissolved in acetone (1 mL, 1.2 mM) and transferred (300  $\mu$ L) into a GC vial, which was placed in a larger vial that contained diethyl ether (3 mL) as a counter solvent. The large vial was stoppered. After a few days quality crystals suitable for X-ray structure determination were obtained by vapor diffusion.

**Details of the crystal structure:** The structure is ordered.  $0.26 \times 0.07 \times 0.02$  mm<sup>3</sup>, orthorhombic, *Pbca*,  $a = 10.95531(15)$ ,  $b = 15.6391(3)$ ,  $c = 32.2937(4)$ ,  $V = 5532.92(15)$  Å<sup>3</sup>,  $Z = 8$ ,  $\mu = 6.46$  mm<sup>-1</sup>,  $T_{min}$ - $T_{max}$ : 0.254-0.886. 28523 reflections were measured up to a resolution of  $(\sin \theta/\lambda)_{max} = 0.617$  Å<sup>-1</sup>. 5427 reflections were unique ( $R_{int} = 0.044$ ), of which 4742 were observed [ $I > 2\sigma(I)$ ]. 380 parameters were refined using 37 restraints.  $R1/wR2$  [ $I > 2\sigma(I)$ ]: 0.035/0.083.  $S = 1.09$ . Residual electron density found between -0.61 and 0.77 e Å<sup>-3</sup>.

### 5.5.5 Density Functional Theory calculations

Electronic structure calculations were performed using DFT, as implemented in the ADF program (SCM). The structures of all possible isomers of [2]<sup>+</sup> and [4]<sup>+</sup> were optimized in water using COSMO to simulate the effect of the solvent. The PBE0 functional and a triple- $\zeta$  potential basis set (TZP) were used for all calculations.

## 5.6 References

1. S. H. Wadman, J. M. Kroon, K. Bakker, M. Lutz, A. L. Spek, G. P. M. van Klink and G. van Koten, *Chem. Commun.*, **2007**, 1907-1909.
2. P. G. Bomben, K. C. D. Robson, P. A. Sedach and C. P. Berlinguette, *Inorg. Chem.*, **2009**, 48, 9631-9643.
3. L. Leyva, C. Sirlin, L. Rubio, C. Franco, R. Le Lagadec, J. Spencer, P. Bischoff, C. Gaiddon, J.-P. Loeffler and M. Pfeffer, *Eur. J. Inorg. Chem.*, **2007**, 3055-3066.
4. H. Huang, P. Zhang, H. Chen, L. Ji and H. Chao, *Chem. - Eur. J.*, **2015**, 21, 715-725.
5. L. Fetzer, B. Boff, M. Ali, M. Xiangjun, J.-P. Collin, C. Sirlin, C. Gaiddon and M. Pfeffer, *Dalton Trans.*, **2011**, 40, 8869-8878.
6. B. Pena, A. David, C. Pavani, M. S. Baptista, J.-P. Pellois, C. Turro and K. R. Dunbar, *Organometallics*, **2014**, 33, 1100-1103.
7. C. Kreitner and K. Heinze, *Dalton Trans.*, **2016**, 45, 13631-13647.
8. J.-P. Collin, M. Beley, J.-P. Sauvage and F. Barigelletti, *Inorg. Chim. Acta*, **1991**, 186, 91-93.

## Chapter 5

9. D. V. Pinnick and B. Durham, *Inorg. Chem.*, **1984**, 23, 1440-1445.
10. L. Salassa, C. Garino, G. Salassa, R. Gobetto and C. Nervi, *J. Am. Chem. Soc.*, **2008**, 130, 9590-9597.
11. P. S. Wagenknecht and P. C. Ford, *Coord. Chem. Rev.*, **2011**, 255, 591-616.
12. J.-P. Collin, D. Jouvenot, M. Koizumi and J.-P. Sauvage, *Inorg. Chem.*, **2005**, 44, 4693-4698.
13. P. Mobian, J.-M. Kern and J.-P. Sauvage, *Angew. Chem.*, **2004**, 116, 2446-2449.
14. B. A. Albani, B. Pena, K. R. Dunbar and C. Turro, *Photochem. Photobiol. Sci.*, **2014**, 13, 272-280.
15. A. M. Palmer, B. Pena, R. B. Sears, O. Chen, M. El Ojaimi, R. P. Thummel, K. R. Dunbar and C. Turro, *Philos. Trans. R. Soc., A*, **2013**, 20120135.
16. J. A. Cuello-Garibo, M. S. Meijer and S. Bonnet, *Chem. Commun.*, **2017**, 53, 6768-6771.
17. S. Fernandez, M. Pfeffer, V. Ritleng and C. Sirlin, *Organometallics*, **1999**, 18, 2390-2394.
18. B. Boff, M. Ali, L. Alexandrova, N. Á. Espinosa-Jalapa, R. O. Saavedra-Díaz, R. Le Lagadec and M. Pfeffer, *Organometallics*, **2013**, 32, 5092-5097.
19. A. D. Ryabov, R. Le Lagadec, H. Estevez, R. A. Toscano, S. Hernandez, L. Alexandrova, V. S. Kurova, A. Fischer, C. Sirlin and M. Pfeffer, *Inorg. Chem.*, **2005**, 44, 1626-1634.
20. B. Peña, N. A. Leed, K. R. Dunbar and C. Turro, *J. Phys. Chem. C*, **2012**, 116, 22186-22195.
21. R. Arakawa, S. Tachiyashiki and T. Matsuo, *Anal. Chem.*, **1995**, 67, 4133-4138.
22. L. Zayat, O. Filevich, L. M. Baraldo and R. Etchenique, *Philos. Trans. R. Soc., A*, **2013**, 371.
23. E. Reisner, T. C. Abikoff and S. J. Lippard, *Inorg. Chem.*, **2007**, 46, 10229-10240.
24. G. M. Sheldrick, *Acta Crystallogr., Sect. A: Found. Adv.*, **2008**, 64, 112-122.